J Solid State Electrochem (2010) 14:465–477
DOI 10.1007/s10008-009-0899-x

ORIGINAL PAPER

Identification of naphthoquinonic and anthraquinonic dyes via sequential potential steps applied to the voltammetry of microparticles methodology

Antonio Doménech-Carbó · María Teresa Doménech-Carbó · Marina Calisti · Vincenzo Maiolo

Received: 17 June 2009 / Revised: 25 June 2009 / Accepted: 26 June 2009 / Published online: 11 July 2009

Abstract An electrochemical method for identifying anthraquinonic, naphthoquinonic, and related dyes in microsamples is reported. This method is based on the sequential application of oxidative and reductive constant-potential polarization steps coupled with the record of square wave voltammograms to solid microsamples of dyes in contact with aqueous electrolytes. As a result, oxidized/reduced products form a layer on the lateral faces of the dye crystals as suggested by attenuated total reflectance-Fourier transform infrared spectroscopy and atomic force microscopy data. This methodology is applied for characterizing alizarin, purpurin, and natural dyes aloe, cochineal red, madder lake, kermes, shellac, and henna attached to paraffin-impregnated graphite electrodes in contact with aqueous potassium phosphate buffer.

Keywords Voltammetry of microparticles · Anthraquinonic dyes · Naphthoquinonic dyes · Polarization steps · Conservation and restoration

Introduction

Anthraquinonic and naphthoquinonic compounds have been widely used as dyeing materials, entering into the composition of painting layers in a variety of works of art and archaeological pieces [1, 2]. Dye identification plays an essential role in the scientific examination of works of art performed in the context of archaeometry, conservation, and restoration. Available methods are conditioned by the need to use minimal amounts of sample (at the microgram level or less), the high dilution of the pigmenting components in the matrix, and the simultaneous presence of dyes, pigments, minerals, binders, and other materials. Recently reported analytical methods for studying dyes in historical paints involve mild extraction by hydrofluoric acid preceding high-performance liquid chromatography (HPLC) [3, 4] and postcolumn deprotonation and complexation with $ZrOCl_2$ HPLC [5].

In the last decades, electrochemical methods have been applied for analyzing dyes in solution phase having different chromophores [6], including anthraquinone [7–9], azo [10–12], and reactive dyes [13, 14]. Additionally, the electrochemistry of anthraquinonic dyes has received attention in relation with "green chemistry" vat dyeing [15, 16] and their use as mediators for the indirect cathodic reduction of dispersed organic compounds [17–19].

Specific constraints arising in dye identification in the fields of conservation and restoration have motivated the development of solid-state electrochemical methods for analyzing dyes in work of art samples [20]. These are based on the voltammetry of microparticles, a methodology tailored by Scholz et al. [21–23], which enables for a highly sensitive record of the electrochemical response of solid materials. Following the seminal work of Scholz et al. on the identification of organic solids [24], this methodology has been previously applied for the identification of anthraquinonic and naphthoquinonic [25, 26], flavonoid [25, 27], and curcumoid [28] dyes in work of art and ancient textile samples, as well as indigo characterization in

A. Doménech-Carbó (✉) · M. Calisti · V. Maiolo
Departament de Química Analítica, Universitat de València,
Dr. Moliner, 50,
46100 Burjassot, València, Spain
e-mail: antonio.domenech@uv.es

M. T. Doménech-Carbó
Departament de Conservació i Restauració,
Universitat Politécnica de València,
Camí de Vera 14,
46022 València, Spain

Maya Blue [29–31]. These works deal with the voltammetry of organic microparticles, which has been studied by several authors [32–35] and can be described within the theoretical models developed by Lovric, Scholz, Oldham, and coworkers [36–40] for the so-called ion-insertion solids.

It is reported here an electrochemical procedure for dye identification in solid microsamples using the voltammetry of microparticles approach. This method consists of the sequential record of the square wave voltammetric responses of solid samples in contact with an aqueous electrolyte before and after the application of oxidative and reductive polarization steps. This procedure extends prior works [25, 27, 28] and is devoted to improve the diagnostic criteria for electrochemically identifying the most frequently used anthraquinone and naphthoquinone dyes, namely alizarin, purpurin, and natural dyes aloe, cochineal red, madder lake, kermes, shellac, and henna. Aloe is actually a mixture of aloine and emodine, while madder lake is a mixture of alizarin, purpurin, and pseudopurpurin. Henna is composed by a mixture of two naphthoquinones, lawsone and juglone. Shellac consisted of a mixture of laccaic acids, whereas kermes and cochineal red are constituted, respectively, by kermesic acid and carminic acid, as coloring components. The structure of such compounds is depicted in Scheme 1.

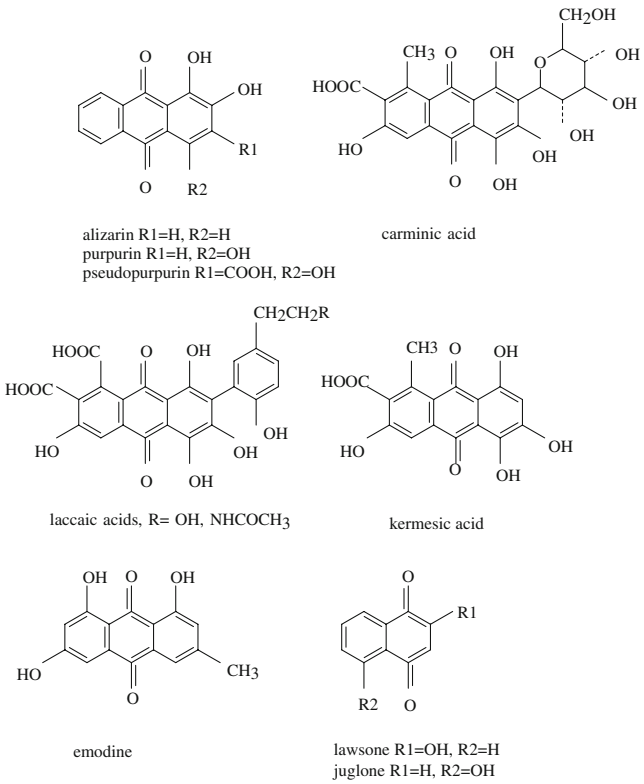

Scheme 1 Schematic representation of the quinone-type compounds in natural dyes involved in this study

Square wave voltammetry was used as a detecting technique by its high sensitivity and immunity to capacitive effects. This technique, whose theory for immobilized reactants was developed by Lovric, Komorsky-Lovric, and Bond [41, 42], is of interest with regard the electrochemistry of solids [43]. Complementary chronoamperometric experiments were performed in order to obtain more detailed information on the involved electrochemical processes [44]. Atomic force microscopy (AFM) and attenuated total reflectance-Fourier transform infrared spectroscopy (ATR-FTIR) experiments, coupled with electrochemical turnovers, were used for studying possible mechanisms involved in electrochemical processes, developing preliminary results [45].

Experimental

Synthetic alizarin (1,2-dihydroxy-9,10-anthraquinone; Sigma) and purpurin (1,2,4-trihydroxy-9,10-anthraquinone; Sigma) were used as reference materials. Carmine (cochineal type from *Coccus cacti* insect) was supplied from AP Fitzpatrick. Shellac from *Coccus lacca* (K 36020), red henna (K 37500), aloe (K 38010), and madder lake (K 37202) were Kremer pigments. Potassium phosphate buffer of 0.50 M (Panreac) was used as a supporting electrolyte.

Paraffin-impregnated graphite electrodes (PIGEs) consist on cylindrical rods of 5 mm diameter of graphite impregnated under vacuum by paraffin [21–23]. To prepare dye-modified PIGEs, 0.1–1 mg of the material was powdered in an agate mortar and pestle and placed on a glazed porcelain tile forming a spot of finely distributed material and then abrasively transferred to the surface of a PIGE by rubbing the electrode over that spot of sample.

Electrochemical experiments were performed at 298 K in a three-electrode cell under argon atmosphere using a AgCl (3 M NaCl)/Ag reference electrode and a platinum-wire auxiliary electrode. Cyclic (CVs) and square wave voltammograms (SQWVs) were obtained with a CH 420I equipment. SQWVs at dye-modified PIGEs were performed on initiating the potential scan either at +1.25 and −0.85 V using a potential step increment of 4 mV and a square wave amplitude of 25 mV. The frequency was varied from 2 to 200 Hz. Linear scan voltammograms and CVs were performed at potential scan rates ranging between 20 and 500 mV/s. Polarization steps were performed by applying potentials of −1.50 or +1.50 V during times between 2 and 15 min to freshly modified electrodes. After this polarization step, detection scans are performed using the conditions described in the above paragraph.

ATR-FTIR spectra were obtained with a Perkin Elmer BX Spectrum Fourier transform infrared spectrometer. Number of co-added scans was 24; resolution was

4 cm^{-1}. Spectra were obtained at fluorine-doped tin oxide electrodes (FTOs; Flexitec) covered by microparticulate deposits of alizarin, dried in air, before and after applying different potential steps in contact with phosphate buffer.

A multimode AFM (Digital Instruments VEECO Methodology Group) with a NanoScope IIIa controller and equipped with a J-type scanner (maximum scan size of 150×150×6 μm) was used. The topography of the samples was studied in contact mode. An oxide-sharpened silicon nitride probe Olympus, VEECO Methodology Group, model NP-S has been used with a V-shaped cantilever configuration. The spring constant is 0.06 N/m and the tip radius of curvature is 5–40 nm. For electrochemical measurements, the AFM was coupled to a Digital Instruments universal bipotentiostat (VEECO Methodology Group). All measurements were performed at room temperature in solutions previously deaerated with argon during 15 min.

Results and discussion

Electrochemical mechanism

Figure 1 shows typical CVs initiated at the open circuit potential (a) in the negative and (b) in the positive direction of potentials. In both cases, a prominent reduction peak is obtained at −0.65 V (I) during the first cathodic scan, but upon repetitive cycling the potential, weaker couples at ca. +0.40 (II), −0.15 (III), and −0.30 V (IV) are recorded. SQWVs for alizarin-modified PIGEs immersed into phosphate buffer are shown in Fig. 2. On scanning the potential from +1.25 V in the negative direction, two overlapping cathodic waves appear at −0.15 and −0.30 V (III and IV, respectively), followed by a sharp peak at −0.65 V (I), as can be seen in Fig. 2a. On scanning the potential from −0.85 V in the positive direction (Fig. 2b), a prominent signal at −0.65 V (I) is accompanied by an isolated peak at +0.40 V (II). Peaks at −0.15 and −0.35 V are enhanced at

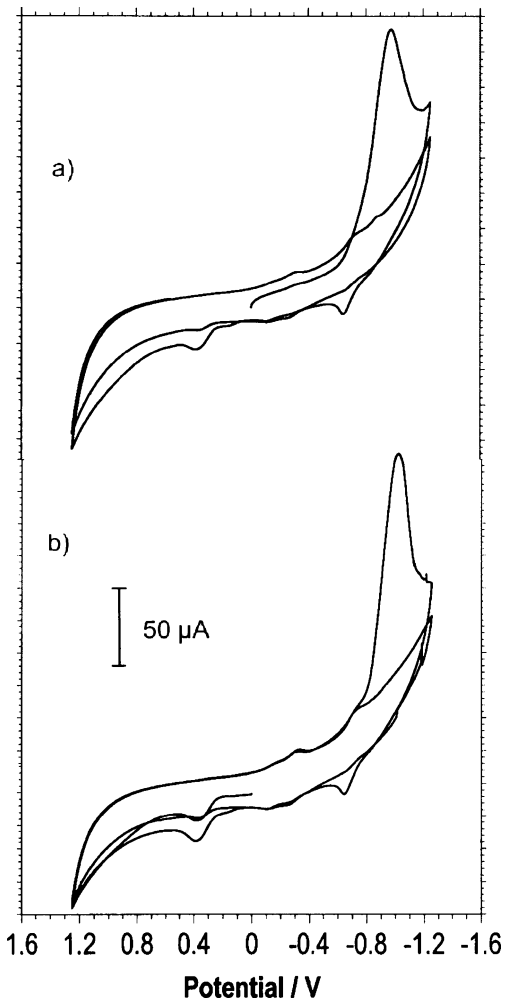

Fig. 1 CVs for alizarin-modified PIGEs immersed into 0.50 M potassium phosphate buffer (pH 7.0). *a* Initial cathodic scan; *b* initial anodic scan. Potential scan rate 50 mV/s

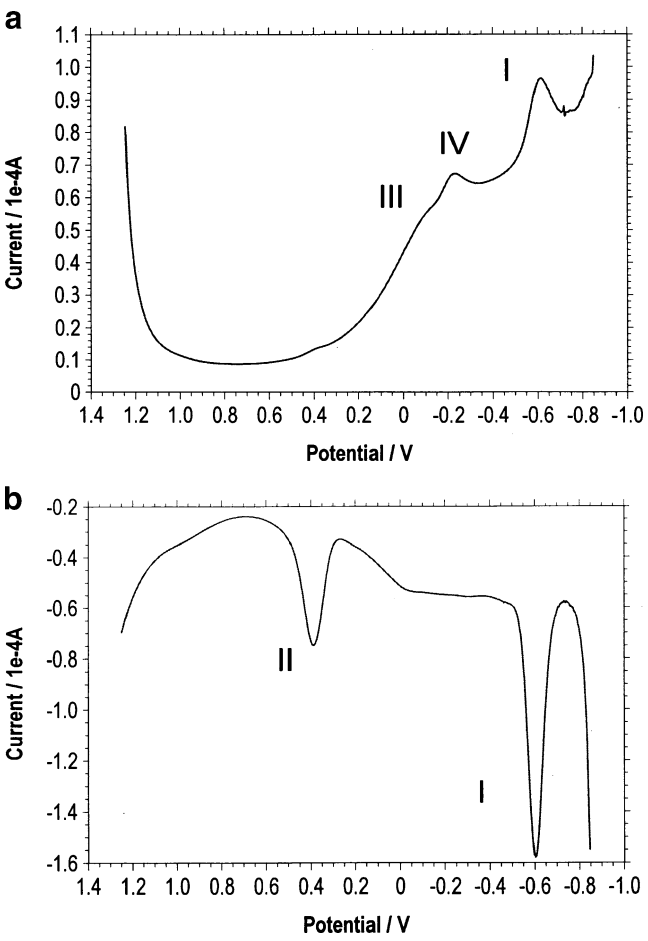

Fig. 2 SQWVs for alizarin-modified PIGEs immersed into 0.50 M potassium phosphate buffer (pH 7.0). Potential initiated at **a** +1.25 V in the negative direction, **b** −0.85 V in the positive direction. Potential step increment 4 mV; square wave amplitude 25 mV; frequency 5 Hz

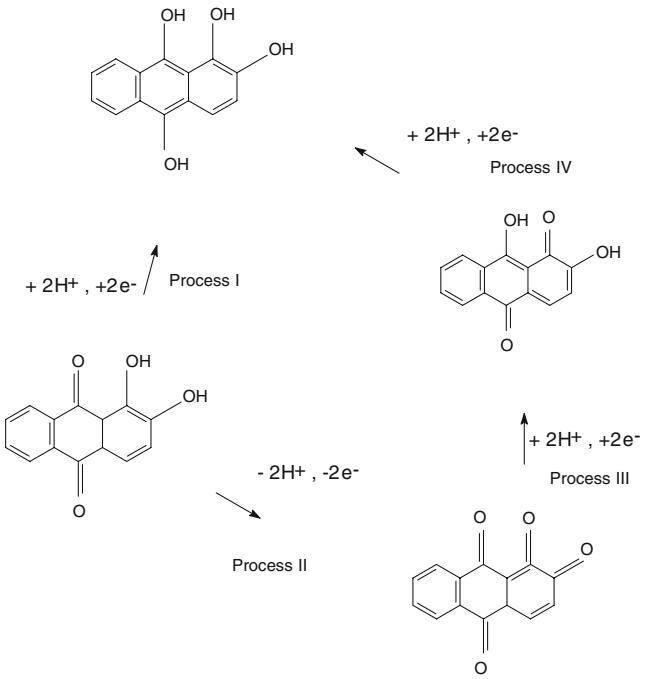

Scheme 2 Main processes involved in solid-state electrochemistry of alizarin

the expense of the reduction peak at −0.60 V after applying a constant potential step of +0.50 V, thus suggesting that such peaks correspond to the reduction of species generated during the electrochemical oxidation process at +0.40 V.

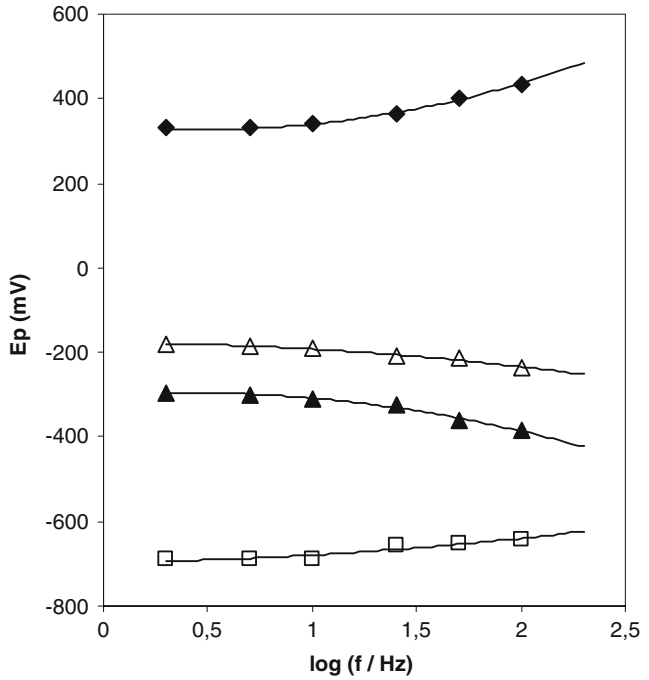

Fig. 3 Variation of peak potentials with frequency for SQWVs of alizarin-modified PIGEs immersed into 0.50 M potassium phosphate buffer (pH 7.0). Potential step increment 4 mV; square wave amplitude 25 mV

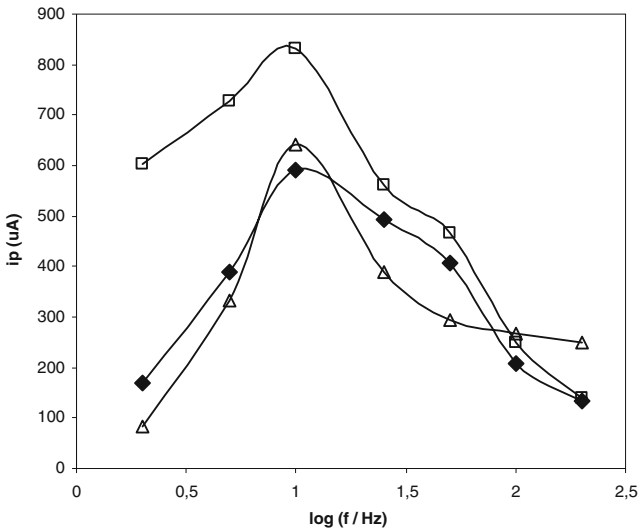

Fig. 4 Variation of peak current with square wave frequency for processes I (*squares*), II (*rhombs*), and III plus IV overlapping peaks (*triangles*). From SQWVs of alizarin-modified PIGEs immersed into 0.50 M potassium phosphate buffer (pH 7.0). Potential step increment 4 mV; square wave amplitude 25 mV

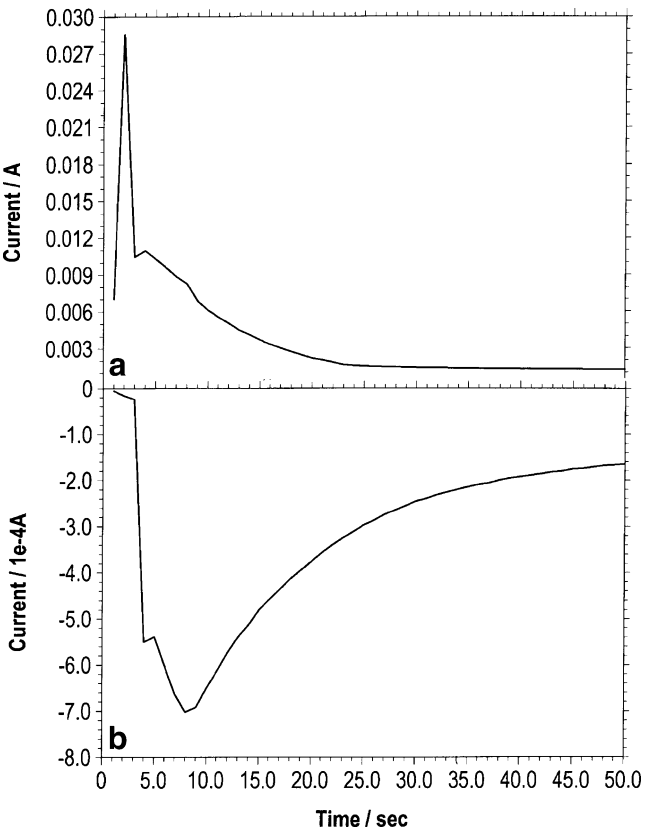

Fig. 5 Current–time curves recorded for microparticulate deposits of alizarin on PIGE electrodes immersed into 0.50 M potassium phosphate buffer (pH 7.0) at applied potentials of **a** −1.0, **b** +0.75 V

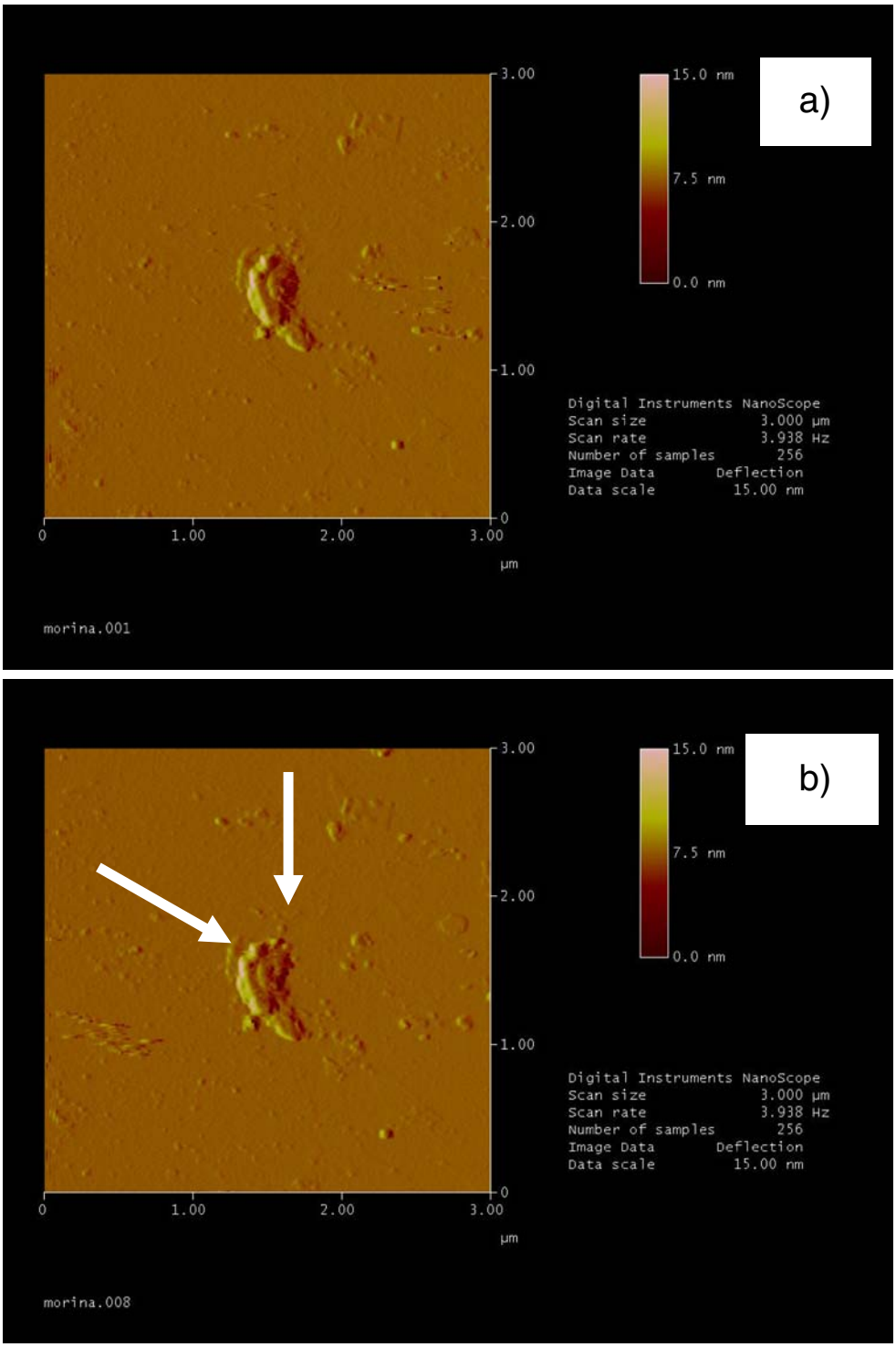

Fig. 6 AFM images of alizarin crystals adhered to a graphite plate in contact with 0.50 M aqueous potassium acetate buffer before (**a**) and after (**b**) application of a linear potential scan between 0.00 and −1.0 V at a sweep rate of 10 mV/s

On considering literature data for the electrochemistry of anthraquinonic dyes in solution phase [46–55], the reduction process at −0.65 V can be described in terms of a two-electron two-proton reversible reduction of the quinone group of the parent alizarin [25, 26], whereas the peak at +0.40 V can be attributed to the oxidation of the *o*-phenol moiety [25, 26], both schematized in Scheme 2. This oxidation process leads presumably to a biquinone species which in turn can undergo different reduction steps to yield the corresponding phenolic derivatives.

The variation of peak potentials with square wave frequency is depicted in Fig. 3. Peaks I and II are positively shifted on increasing square wave frequency, whereas peaks III and IV are negatively shifted on increasing frequency.

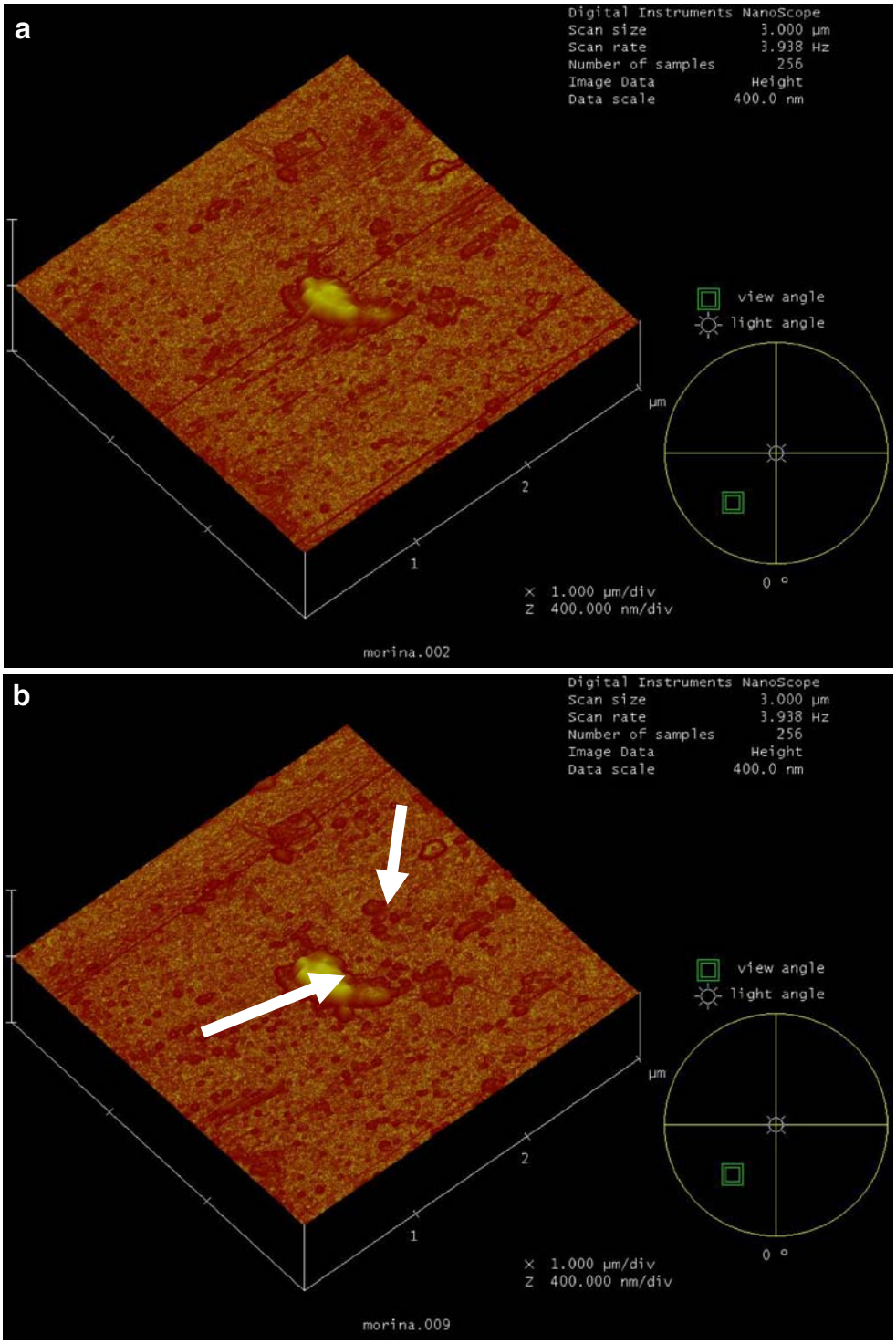

Fig. 7 Topographic AFM images of alizarin crystals adhered to a graphite plate in contact with 0.50 M aqueous potassium acetate buffer before (**a**) and after (**b**) application of a linear potential scan between 0.00 and +1.0 V at a sweep rate of 10 mV/s

On first examination, this behavior can be interpreted in terms of the appearance of kinetic complications, presumably the involvement of a chemical reaction succeeding processes I and II or preceding (peaks III and IV) the electron transfer process. Remarkably, the variation of peak current on square wave frequency for these electrochemical processes suggests a possibly complicated pathway. As shown in Fig. 4, at square wave frequencies below 50 Hz, the peak current increases on increasing frequency; however, at frequencies above 50 Hz, the peak current decreases on increasing frequency. These features suggest that the electrochemical process proceeds initially via proton insertion/issue coupled with electron transfer. Subsequent progress of the electrochemical reaction across the

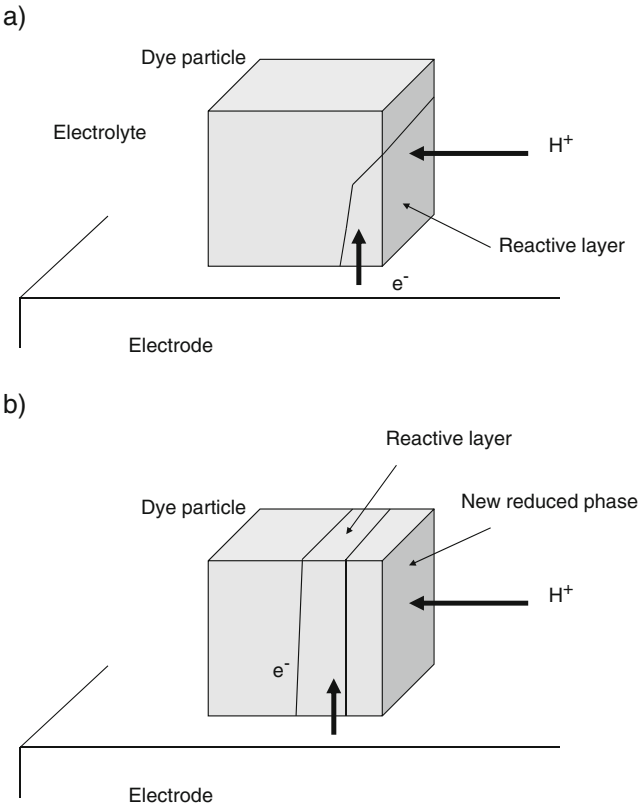

Fig. 8 **a**, **b** Scheme for the description of the solid-state electrochemical reduction of an organic dye via concerted proton- and electron-transfer processes in two successive steps

crystal probably involves formation of a new phase constituted by the reduced or oxidized material partially covering the lateral faces of the parent crystal, as previously suggested [45].

This voltammetry can be rationalized on the basis of the theoretical models developed by Lovric, Scholz, Oldham, and coworkers [36–40]. In the case of insoluble organic compounds able to undergo proton-exchange reactions with the electrolyte, the surface reactions initially occurs on the particle/electrode/electrolyte interface. From there, the redox reaction expands over the surface and into the body of the particle. Here, charge transport occurs via proton hopping and electron hopping between adjacent molecules in the solid. It should be emphasized that charge conservation requires the simultaneous ingress (or issue) of electron and protons in the solid particles in reduction (or oxidation) processes. Analysis of chronoamperometric data for different dyes using the aforementioned model indicated that proton hopping is slower than electron hopping in organic solids [44]. As a result, proton-assisted reduction and oxidation processes should be localized in a shallow layer in the vicinity of the particle/electrolyte interface, in agreement with expectances from the Lovric and Scholz model with significantly restricted proton diffusion across the solids.

Chronoamperometric data at potentials of +0.55 and −0.85 V using experiment times between 10 and 100 ms produced results in agreement with the above theoretical predictions [36–40], thus allowing for an estimate of the values for the diffusion coefficients of protons (D_H) and electrons (D_e) in dye crystals. In contact with potassium phosphate buffer, D_H values of 2×10^{-10} cm^2/s and D_e values of 8×10^{-7} cm^2/s were obtained in agreement with previously reported data [44]. Remarkably, the effective breadth of the electroactive layer, d, was estimated between 20 to 70 nm, in agreement with the mean thickness of the reaction layer recorded in AFM images (*vide infra*).

The electrochemical mechanism at longer times, however, is probably more complicated, as suggested by long-time chronoamperometric experiments. As shown in Fig. 5 for the reduction of alizarin at −1.0 V (a) and its oxidation at +0.75 V (b), the initial current decrease is interrupted by a transient current growth, in turn followed by a current decrease. This situation parallels that existing in, for instance, nucleation processes in the electrodeposition of quinolein derivatives on mercury electrodes [56, 57] and layer-by-layer electrodeposition processes [58, 59], thus suggesting that the formation of a new phase is involved.

In situ AFM images of crystals of alizarin, monitored during the course of their solid-state electrochemical oxidation/reduction in contact with aqueous acetate buffer, are consistent with the above expectances. Figure 6 shows in situ AFM images from the upper face and sides of crystals of alizarin (a) before and (b) after application of a linear potential step between 0.0 and −1.0 V. Here, an agglomerate of crystals of ca. 1×0.5 μm exhibits significant changes during the potential scan, consisting of the apparent growth of several crystals (arrow). The maximum extent of the distortions of crystals can be estimated as ca. 50–80 nm. Minor crystal growth features were observed for the application of an oxidative step between 0.0 and +1.0 V (see Fig. 7). The progress of the electrochemical reaction, as judged by morphological changes, was significantly lowered on increasing time, thus denoting that no reductive/oxidative dissolution processes occur under our experimental conditions.

These features can be rationalized on considering that, as described by Hasse and Scholz [60] for in situ AFM examination of the litharge (PbO) to lead metal reduction, one can assume that the reduction of alizarin takes place without morphological disintigration but as a process in which the lateral sides of the initial crystal are continuously shrunk and reconstructed forming a new layer. This suggest that a topotactic process occurs initially, eventually accompanied by exfoliation and restacking [61]. Accordingly, at relatively short times, the advance of the electrochemical reaction through the crystals, involving O–H bond formation, is coupled with the advance of the diffusion front of protons

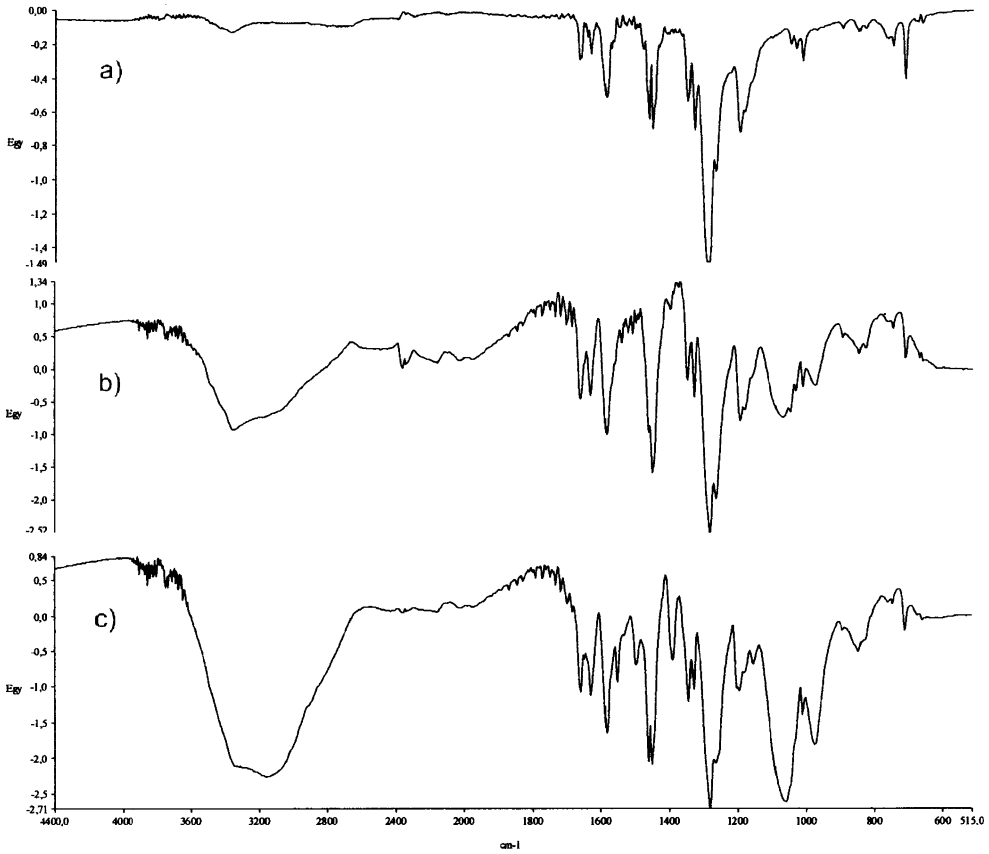

Fig. 9 ATR-FTIR spectra of alizarin-modified FTO electrodes *a* before and *b*, *c* after application of a constant potential step of *b* +1.0 and *c* −1.0 V during 30 min in contact with potassium phosphate buffer

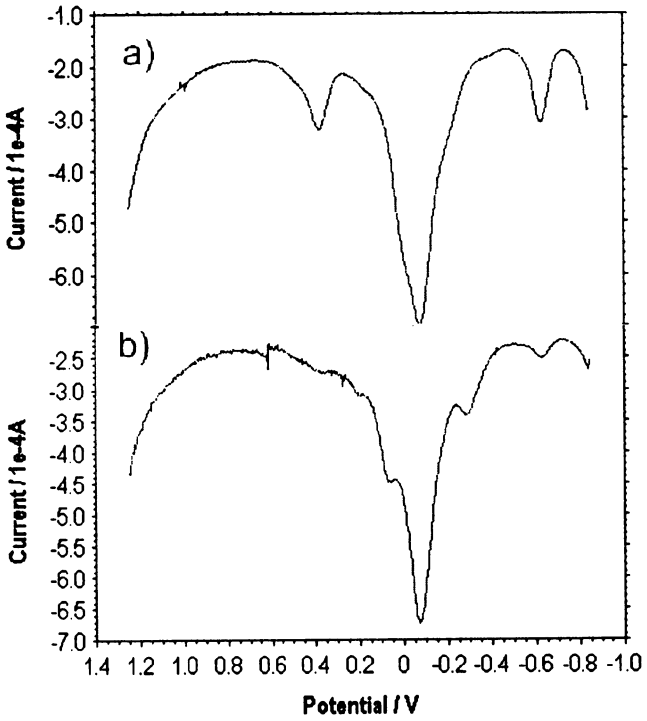

Fig. 10 SQWVs for alizarin-modified PIGEs immersed into 0.50 M phosphate buffer (pH 7.0) after application of a potential step of *a* +1.50 V, potential scan initiated at +1.25 V in the negative direction; *b* −1.50 V, potential initiated at −0.85 V in the positive direction. Potential step increment 4 mV; square wave amplitude 25 mV; frequency 5 Hz

through the crystal. At sufficiently long times, crystal restructuring and formation of a new phase possibly occur, as suggested by CA curves in Fig. 5.

In the case of oxidation, the unique source of protons is the reservoir of –OH groups of the parent alizarin units. Again, the progress of the reaction through the alizarin crystal should involve a significant crystal restructuring and eventually formation of a new diquinone (see Scheme 2) phase. Now, probably there is decoupling between the advance of the quinone/diquinone interface and proton diffusion so that the new phase can act as a blocking layer with regard to proton diffusion. Conjectured phase transitions could, in principle, be taken as a reasonable feature taking into account that the compound resulting from the proton-assisted oxidation or reduction of the parent dye involves a hydrogen bonding system significantly different from that of the pristine compound.

It should be noted that the crystal packing of alizarin can be described in terms of herringbone stacking of molecules, but there is possibility of conformational rearrangements. In fact, it has been reported that anthraflavic acid (2,6-dihydroxyanthraquinone), $C_{14}H_8O_4$, an isomer of the alizarin dye, adopts a planar conformation, with crystallographic *mm* symmetry consisting of superimposed sheets of molecules in a graphite-like structure [62]. Accordingly, it appears reasonable to consider that the structure of alizarin

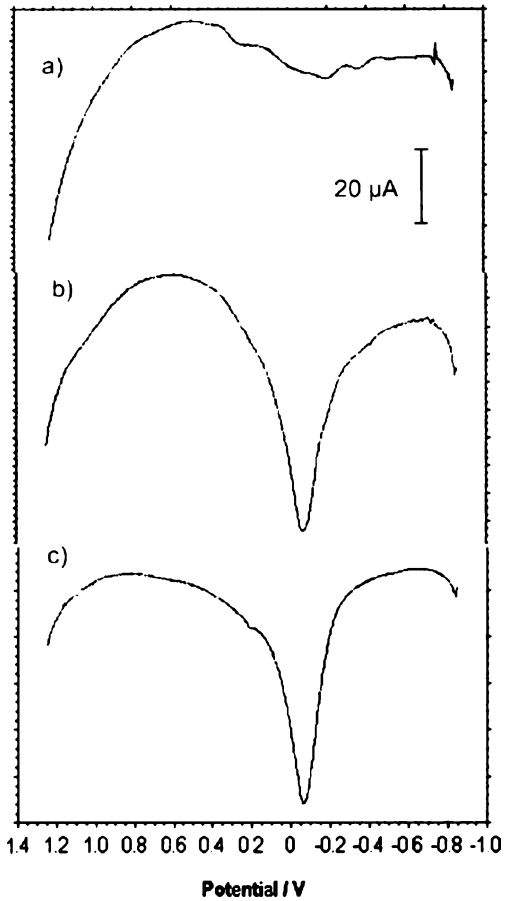

Fig. 11 SQWVs of henna-modified PIGEs immersed in 0.50 M phosphate buffer (pH 7.0). *a* Pristine-modified electrode; *b* id. after application of a potential step of +1.50 V during 10 min; *c* id. after application of a potential step of −1.50 V during 10 min. Potential scan initiated at −0.85 V in the positive direction. Potential step increment 4 mV; square wave amplitude 25 mV; frequency 5 Hz

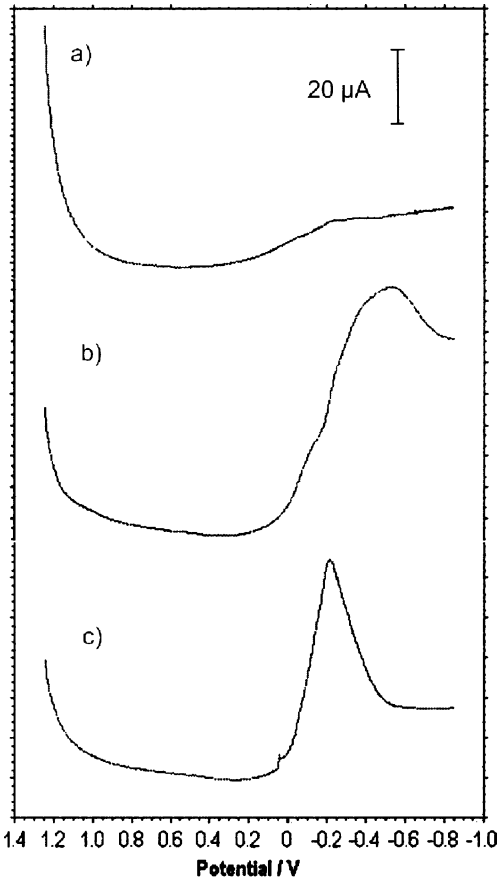

Fig. 12 SQWVs of henna-modified PIGEs immersed in 0.50 M phosphate buffer (pH 7.0). *a* Pristine-modified electrode; *b* id. after application of a potential step of +1.50 V during 10 min; *c* id. after application of a potential step of −1.50 V during 10 min. Potential scan initiated at +1.25 V in the negative direction. Potential step increment 4 mV; square wave amplitude 25 mV; frequency 5 Hz

is sufficiently flexible to admit significant structural changes upon oxidation or reduction. In fact, differences in color between crystals and solutions of anthraquinonic dyes are ascribable to the changes in molecular conformations or to the impact of hydrogen bonds [63]. Additionally, the growth habit of alizarin crystals can be modified by solvent blocking of growth of specific crystal faces in the alcohol solutions [64].

Taking into account the foregoing set of considerations, a tentative scheme for electrochemical reduction of alizarin, in principle able to be extended to similar dyes, could involve (a) coupled insertion of protons and electrons with formation of a layer of reduced molecules with no changes in the crystal structure, (b) advance of the above layer with formation of a new crystalline phase, and (c) depending on the proton permeability of the new phase, blocking of the reduction process or subsequent advance of the new phase and the preceding proton diffusion layer along the crystal. A tentative pictorial representation is depicted in Fig. 8.

ATR-FTIR experiments act in support of the idea that a layer of new compounds is formed during electrochemical oxidation or reduction of alizarin microparticulate deposits. Thus, Fig. 9 compares the spectra for alizarin-modified FTO electrodes (a) before and (b, c) after application of a constant potential step of (b) +1.0 and (c) −1.0 V during 30 min in contact with potassium phosphate buffer. Following recent band assignments [65, 66], the spectrum of alizarin exhibits strong bands at 1,258, 1,296 (ν(CO)/ν(CC)/δ(CCC)), 1,452, and 1,478 cm^{-1} (ν(CC)/δ(COH)/δ(CCC)) accompanying the carbonyl stretch band at 1,633 cm^{-1}. Remarkably, the region of OH stretch at ca. 3,400 cm^{-1} exhibits weak bands. Upon electrochemical reduction, the spectrum changes significantly, the OH bands around 3,200 cm^{-1} being remarkably enhanced and broadened, an effect associated to hydrogen bond formation, while the morphology of 1,258/1,296 and 1,452/1,478 cm^{-1} bands becomes modified whereas a new band at 1,395 cm^{-1} (ν(CC)/δ(CH)) is recorded. Upon oxidative treatment, OH bands become slightly increased with respect

Table 1 Peak potential data (mV vs. AgCl/Ag) recorded in the initial potential scan of freshly prepared dye-modified PIGEs (a) before and (b) after applying a reductive potential step of −1.50 V during 10 min

Dye	E_p (a1)	E_p (b1)	E_p (a2)	E_p (b2)
Alizarin	−225 −610[a]	+395[a] −600[a]	−200[a] −630	+605 −290 −715[a]
Henna	−225	+250 −525	−210[a]	−620[a]
Shellac	−210[a]	−650[a]	−210[a]	−590[a]
Purpurin	+300 −260	+295[a] −620	−225[a] −550[a]	+225 −215[a] −560[a]
Madder	−180 −685	+685 −300	+160 −295	+205 −715[a]
Cochineal red	−290 −715	+235 −720[a]	−320	+205 −430
Kermes	−345 −695	+220 −695	−540	+190

Electrolyte: 0.50 M potassium phosphate buffer, pH 7.0. (1) Potential scan initiated at +0.85 V in the negative direction; (2) potential scan initiated at −0.85 V in the positive direction. Potential step increment 4 mV; square wave amplitude 25 mV; frequency 15 Hz

[a] Strong peaks

to those recorded for the parent alizarin. Bands at 1,047, 1,031, and 1,012 cm^{-1} (δ(CCC); ν(CC)/δ(CH); ν(CC)/δ(CCC)) become significantly but similarly modified both upon oxidation and reduction. In contrast, 1,198 and 1,161 cm^{-1} (ν(CC)/δ(CH)/δ(CCC)) remain unaltered upon oxidation but change (with a new band at 1,140 cm^{-1}) upon reduction. These features are in principle consistent with the reaction pathway illustrated in Scheme 2.

Analytical performance

The foregoing data suggest that proton-assisted reduction and oxidation processes involving microparticulate deposits of organic dyes are localized in a shallow layer in the vicinity of the particle/electrolyte interface, in agreement with expectances from the Lovric and Scholz model with significantly restricted proton diffusion across the solids [44, 45]. Within this scheme, one can expect that application of a constant potential at high negative or positive potentials should produce significant changes in the voltammetric response. In short, the idea is that at least a surface region of the particles will be converted into the oxidation or reduction product, as previously discussed. Then, a subsequent potential scan should permit to record the response of that compound, thus increasing the disposable diagnostic criteria for identifying the parent compound.

This can be seen in Fig. 10, where the SQWVs of alizarin-modified PIGEs after application of polarization steps of (a) +1.50 V and (b) −1.50 V during 10 min are shown. Remarkably, the voltammetric record changes significantly. After the application of the oxidative polarization, the peak at −0.60 V corresponding to the reduction of alizarin disappears, being replaced by a prominent reduction signal at −0.20 V (Fig. 10 a). After the application of the reductive polarization step, the alizarin peaks at +0.40 and −0.60 V also disappear, being replaced by a accompanied by a prominent peak consisting of overlapping signals at −0.20, −0.08, and +0.06 V (Fig. 10 b). This relatively complex voltammetry derives from the formation of different quinone/hydroquinone products during electrochemical turnovers. The appearance of

Table 2 Peak potential data (mV vs. AgCl/Ag) recorded in the initial potential scan of freshly prepared dye-modified PIGEs (a) before and (b) after applying an oxidative potential step of +1.50 V during 10 min

Dye	E_p (a1)	E_p (b1)	E_p (a2)	E_p (b2)
Alizarin	−225 −610[a]	+395[a] −600[a]	−230[a] −630	+383 −625 −715[a]
Henna	−225	+250 −525	−525	−620[a]
Shellac	−210[a]	−650[a]	−565	+170
Purpurin	+300 −260	+295[a] −620	+310 −360 −710[a]	+285[a] +214[a] −650
Madder	−180 −685	+685 −300	−525	+675 +365
Cochineal red	−290 −715	+235 −720[a]	+235 −545[a]	+235 −715
Kermes	−345 −695	+220 −695		+210

Electrolyte: 0.50 M potassium phosphate buffer, pH 7.0. (1) Potential scan initiated at +0.85 V in the negative direction; (2) potential scan initiated at −0.85 V in the positive direction. Potential step increment 4 mV; square wave amplitude 25 mV; frequency 15 Hz

[a] Strong peaks

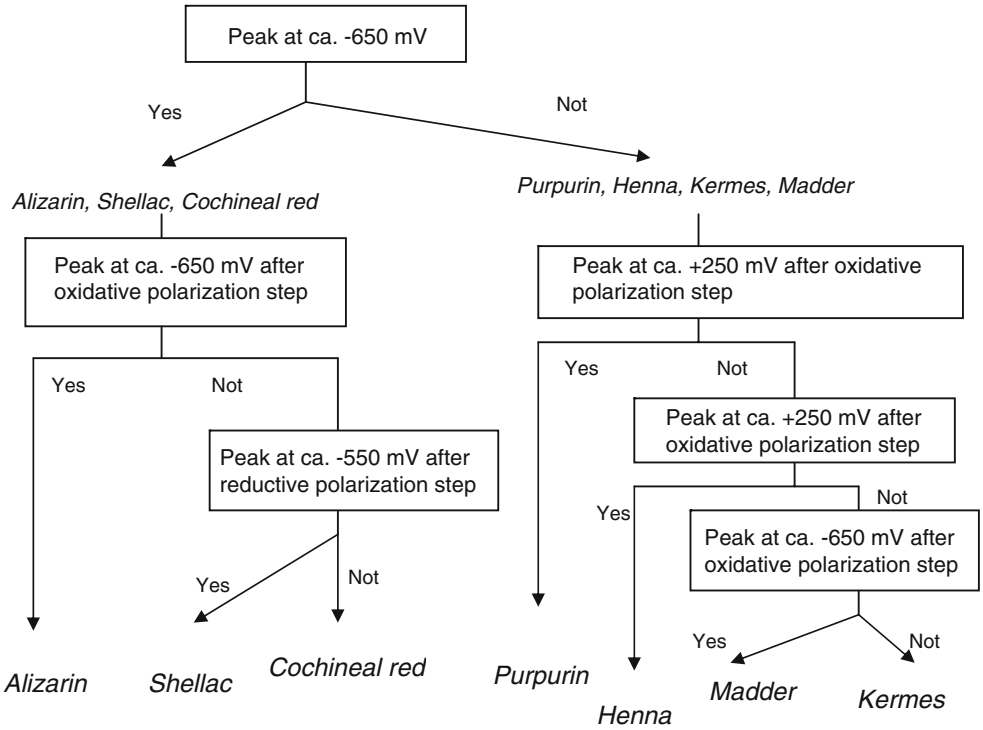

Fig. 13 Identification scheme for anthraquinonic dyes in contact with potassium phosphate buffer using square wave voltammograms initiated at −0.85 V in the positive direction

multiple peak profiles can be considered as consistent with the observations of Grygar et al. [26] and Dai and Shin [46] concerning the sensibility of anthraquinone electrochemistry to the application of different polarization steps. Studies of anthraquinonic and phenolic compounds in solution phase reveals that the electrochemical response is sensitive to kinetic effects yielding secondary products [46–55]. In particular, polyhydroxy compounds can produce electrochemical oxidations with a cascade mechanism, the final oxidation product being nonelectroactive [55].

From our purposes, the relevant point to emphasize is that the application of oxidative and reductive polarization

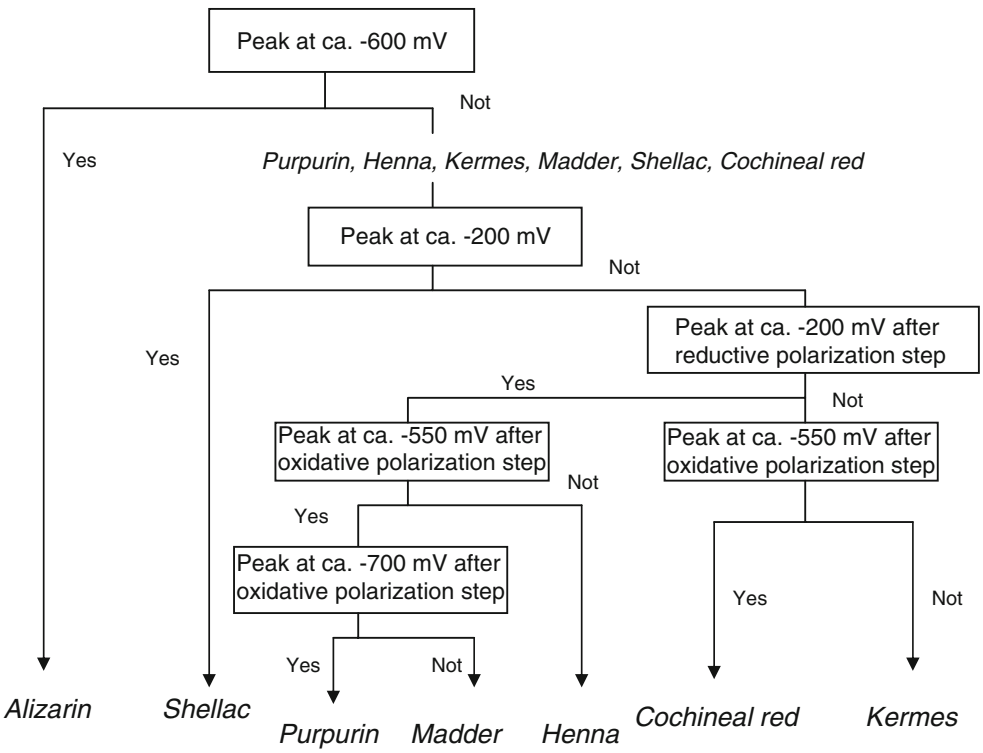

Fig. 14 Identification scheme for anthraquinonic dyes in contact with potassium phosphate buffer using square wave voltammograms initiated at +0.85 V in the negative direction

steps is able to enhance the analytical performance for the electrochemical recognition of the studied dyes, as can be seen in the case of henna. Thus, Fig. 11 compares the SQWVs of henna-modified PIGEs initiated at −0.85 V in the positive direction (a) without application of any potential step, (b) after application of a potential step of +1.50 V, and (c) after application of a potential step of −1.50 V, both during 10 min. Whereas the voltammogram of the pristine product produced no marked peaks, the postpolarization voltammograms yield a prominent peak at −0.08 V. A similar situation was obtained in SQWVs initiated at +1.25 V in the negative direction, depicted in Fig. 12. Again, the pristine material produces a poorly defined response whereas the postpolarization voltammograms give intense peaks.

It should be noted that, even in the case of dyes displaying marked voltammetric responses, the use of data for postpolarization voltammograms increases the number of parameters able to be used for identification with respect to the use of pristine material alone. Obtained results for the studied anthraquinonic and naphthoquinonic dyes are summarized in Tables 1 and 2. For practical purposes, however, it should be noted that, in real samples from works of art, matrix effects can distort significantly the observed voltammetric response. Accordingly, it is convenient to design analytical protocols based on the recognition of the most prominent voltammetric signals. Using electrochemical data in Tables 1 and 2, one can propose different identification sequences based, solely, in strong peaks in voltammograms recorded at dye-modified electrodes. Figure 13 shows an identification scheme for anthraquinonic dyes in contact with potassium phosphate buffer using square wave voltammograms initiated at −0.85 V in the positive direction. Combination of data for initial voltammograms and for voltammograms recorded after oxidative and reductive polarization steps provides a procedure for identifying each one of the dyes. A similar scheme using square wave voltammograms initiated at +0.85 V in the negative direction is depicted in Fig. 14.

Conclusions

Both the electrochemical reduction and oxidation of microparticulate deposits of alizarin immersed into aqueous phosphate buffer lead to the formation of a layer of new reduced or oxidized products displaying well-defined ATR-FTIR spectra. Such new products form a layer covering lateral faces of pristine crystals, as suggested by AFM data.

Consistently, application of constant potential polarization steps results in significant modifications of the voltammetric response of anthraquinonic and naphthoquinonic dyes attached to PIGEs in contact with aqueous phosphate buffer. As a result, dye-characteristic responses, able to be interpreted in terms of current models in solid-state voltammetry of immobilized microparticles, are obtained.

The reported methodology enhances the sensitivity of dye recognition via solid-state electrochemistry and enhances the number of parameters usable as diagnostic criteria for identifying dyes. This is potentially interesting in the analysis of work of art samples, where high dilution of pigmenting compounds and possible interfering compounds is difficult significantly in dye identification.

Acknowledgments Financial support is gratefully acknowledged from the I + D + I MCYT BQU2001-2776-C03-01 and 02 and I + D + I GV04B/197 Projects.

References

1. Mills JS, White R (2001) The organic chemistry of museum objects, 2nd edn. Butterworth-Heinemann, Oxford, pp 121–133
2. Fitzhugh E, Roy A, Feller RL (eds) (1997) Artist's Pigments: a handbook of their history and characteristics. National Gallery of Art, London
3. Sanyova J, Reisse J (2006) J Cult Heritage 7:229
4. Sanyova J (2008) Microchim Acta 162:361
5. Surowiec I, Nowik W, Trojanowicz M (2008) Microchim Acta 162:393
6. Bersier PM, Bersier J (1986) Trends Anal Chem 5:97
7. Almeida PJ, Rodrigues JA, Barros AA, Fogg AG (1999) Anal Chim Acta 385:287
8. Zima J, Barek J, Moreira JC, Mejstrik V, Fogg AG (1999) Crit Rev Anal Chem 29:125
9. Zima J, Barek J, Moreira JC, Mejstrik V, Fogg AG (2001) Fresenius J Anal Chem 369:567
10. Barek J, Thuan HP, Mejstrik V, Moreira JC, Zima J (1998) Anal Lett 31:1219
11. Barek J, Thuan HP, Mejstrik V, Moreira JC, Zima J (1997) Collect Czech Chem Commun 62:597
12. Combeau S, Chatelut M, Vittori O (2002) Talanta 56:115
13. Fogg A, Zanoni MVB, Yusoff ARHM, Ahmad R, Barek J, Zima J (1998) Anal Chim Acta 362:235
14. Barek J, Fogg AG, Moreira JC, Zanoni MVB, Zima J (1996) Anal Chim Acta 320:31
15. Blackburn RS, Harvey A (2004) Environ Sci Technol 38:4034
16. Bozic M, Kokol V (2008) Dyes Pigments 76:299
17. Bechtold T, Burtscher E, Gmeiner D, Bobleter O (1991) J Electroanal Chem 306:169
18. Bechtold T, Burtscher E, Turcanu A (1999) J Electroanal Chem 465:80
19. Vuorema A, John P, Keskitalo M, Kulandainathan MA, Marken F (2008) Dyes Pigments 76:542
20. Doménech A, Doménech MT, Costa V (2009) Electrochemical methods in archeometry, conservation and restoration. Springer, Berlin
21. Scholz F, Meyer B (1998) Voltammetry of solid microparticles immobilized on electrode surfaces. In: Bard AJ, Rubinstein I (eds) Electroanalytical chemistry, a series of advances, vol 20. Marcel Dekker, New York, pp 1–87
22. Grygar T, Marken F, Schröder U, Scholz F (2002) Collect Czech Chem Commun 67:163

23. Scholz F, Schröder U, Gulaboski R (2005) Electrochemistry of immobilized particles and droplets. Springer, Berlin
24. Scholz F, Nitschke L, Henrion G (1989) Fresenius Z Anal Chem 334:56
25. Doménech A, Doménech MT, Saurí MC, Gimeno JV, Bosch F (2003) Anal Bioanal Chem 375:1169
26. Grygar T, Kuckova S, Hradil D, Hradilova D (2003) J Solid State Electrochem 7:706
27. Doménech A, Doménech MT, Saurí MC (2005) Talanta 66:769
28. Doménech A, Doménech MT, Saurí MC (2005) Microchim Acta 152:75
29. Doménech A, Doménech MT, de Agredos Pascual ML Vázquez (2006) J Phys Chem B 110:6027
30. Doménech A, Doménech MT, de Agredos Pascual ML Vázquez (2007) J Phys Chem C 111:4585
31. Doménech A, Doménech MT, de Agredos Pascual ML Vázquez (2007) Anal Chem 79:2812
32. Jaworski A, Stojek Z, Scholz F (1993) J Electroanal Chem 354:1
33. Bond AM, Marken F, Hill E, Compton RG, Hügel H (1997) J Chem Soc Perkin Trans 2:1735
34. Komorsky-Lovric S, Mirceski V, Scholz F (1999) Mikrochim Acta 132:67
35. Komorsky-Lovric S (1997) J Solid State Electrochem 1:94
36. Lovric M, Scholz F (1997) J Solid State Electrochem 1:108
37. Oldham KB (1998) J Solid State Electrochem 2:367
38. Lovric M, Hermes M, Scholz F (1998) J Solid State Electrochem 2:401
39. Lovric M, Scholz F (1999) J Solid State Electrochem 3:172
40. Schröder U, Oldham KB, Myland JC, Mahon PJ, Scholz F (2000) J Solid State Electrochem 4:314
41. Komorsky-Lovric S, Lovric M, Bond ASM (1992) Anal Chim Acta 258:299
42. Komorsky-Lovric S (1995) J Electroanal Chem 397:211
43. Lovric M (2002) In: Scholz F (ed) Electroanalytical methods. Springer, Berlin, p 111
44. Doménech A, Doménech MT (2006) J Solid State Electrochem 10:949
45. Doménech A, Doménech MT (2008) Electrochem Commun 10:1238
46. Dai H-P, Shin K-K (1998) Electrochim Acta 43:2709
47. Amatore C, Lefrou C, Pflüger F (1989) J Electroanal Chem 270:43
48. Garreau D, Hapiot P, Savéant J-M (1990) J Electroanal Chem 289:73
49. Hodnick WF, Milosavljevic EB, Nelson JH, Pardini RS (1988) Biochem Pharmacol 37:2607
50. Hendrickson HP, Kaufman AD, Lunte GE (1994) J Pharmac Biomed Anal 12:325
51. Ciolowski EL, Maness KM, Cahill PS, Wightman RM, Evans DH, Fosset B, Amatore C (1994) Anal Chem 66:3611
52. Shaw SJ, Marken F, Bond AM (1996) Electroanalysis 8:732
53. Petit Chr, Nagy A, Quarin G, Kauffmann JM (1996) J Pharm Belgique 51:1
54. Jovanovich SV, Steenken S, Hara Y, Simic MG (1996) J Chem Soc Perkin Trans 1:2497
55. Brett AMO, Ghica M-E (2003) Electroanalysis 15:1745
56. Müller C, Claret J, Martínez F, Sarret M (1986) J Electroanal Chem 202:203
57. Müller C, Claret J, Sarret M (1987) Electrochim Acta 32:283
58. Rangarajan SK (1973) J Electroanal Chem 46:125
59. Obretenov W, Petrov I, Nachev I, Staikov G (1980) J Electroanal Chem 109:195
60. Hasse U, Scholz F (2001) Electrochem Commun 3:429
61. Feng Q, Kajiyoshi K, Yanagisawa K (2003) Chem Lett 32:48
62. de Ruyk J, Preat J, Perpète EA, Jacquemin D, Wouters J (2006) Acta Cryst E62:4503
63. Yatsenko AV, Chernyshev VV, Popov SI, Sonneveld EJ, Schenk H (2000) Dyes Pigments 45:169
64. Algra RE, Graswinckel WS, van Enckevort VJP, Vlieg E (2005) J Crystal Growth 285:168
65. Cañamares MV, García-Ramos JV, Domingo C, Sánchez-Cortés S (2004) J Raman Spectrosc 35:921
66. Kiel EG, Heertjes PM (2008) J Soc Dyers Colour 79:21